

Effect of composition, annealing temperature, and high pressure torsion on structure and hardness of Ti-V and Ti-V-Al alloys

Cite as: J. Appl. Phys. **125**, 082522 (2019); <https://doi.org/10.1063/1.5053937>

Submitted: 28 August 2018 . Accepted: 24 November 2018 . Published Online: 12 December 2018

Alena S. Gornakova, Alexandr B. Straumal, Igor I. Khodos, Ivan B. Gnesin, Andrey A. Mazilkin, Natalia S. Afonikova, and Boris B. Straumal 



View Online



Export Citation



CrossMark

ARTICLES YOU MAY BE INTERESTED IN

[Magnetic resonance imaging of strain in elastic gels](#)

Journal of Applied Physics **125**, 082521 (2019); <https://doi.org/10.1063/1.5054277>

[Strain effect on band structure of InAlAs digital alloy](#)

Journal of Applied Physics **125**, 082514 (2019); <https://doi.org/10.1063/1.5045476>

[Strain measurement of ultrathin epitaxial films using electron diffraction techniques](#)

Journal of Applied Physics **125**, 082401 (2019); <https://doi.org/10.1063/1.5049357>

Ultra High Performance SDD Detectors



See all our XRF Solutions

Effect of composition, annealing temperature, and high pressure torsion on structure and hardness of Ti-V and Ti-V-Al alloys

Cite as: J. Appl. Phys. **125**, 082522 (2019); doi: [10.1063/1.5053937](https://doi.org/10.1063/1.5053937)

Submitted: 28 August 2018 · Accepted: 24 November 2018 · Published Online: 12 December 2018



Alena S. Gornakova,¹ Alexandr B. Straumal,¹ Igor I. Khodos,^{2,3} Ivan B. Gnesin,¹ Andrey A. Mazilkin,^{1,4}
Natalia S. Afonikova,¹ and Boris B. Straumal^{1,2,4,5,a)} 

AFFILIATIONS

¹Russian Academy of Sciences, Institute of Solid State Physics, Chernogolovka, Russia

²Chernogolovka Scientific Center, Russian Academy of Sciences, Chernogolovka, Russia

³Russian Academy of Sciences, Institute of Microelectronics Technology and High Purity Materials, Chernogolovka, Russia

⁴Karlsruhe Institute of Technology (KIT), Institute of Nanotechnology, Eggenstein-Leopoldshafen, Germany

⁵Department of Chemical Physics, National University of Science and Technology "MISIS," Moscow, Russia

^{a)}Author to whom correspondence should be addressed: straumal@issp.ac.ru

ABSTRACT

The severe plastic deformation strongly changes the microstructure and properties of titanium-based alloys. The structure and microhardness of four binary and ternary titanium-based alloys (Ti-4 wt. % V, Ti-4 wt. % V-6 wt. % Al, Ti-4 wt. % V-3 wt. % Al, and Ti-5 wt. % V-6 wt. % Al) have been studied after preliminary annealing and following high pressure torsion (HPT). After HPT, the Ti-4 wt. % V alloy contains much less (ω Ti) phase than Ti-4 wt. % Fe and Ti-4 wt. % Co alloys. The addition of aluminum to the binary Ti-V alloys completely suppresses the formation of the high-pressure (ω Ti)-phase. HPT leads to the partial decomposition of the annealed (α Ti) solid solution and "purification" of α -phase similar to that in the Ti-Fe alloys. After HPT of the studied ternary alloys, the (β Ti)-phase completely disappears and nanoparticles of Ti₂Fe form instead. This fact explains why the addition of aluminum leads to the increase of microhardness of alloys after annealing between 600 °C and 950 °C and after HPT-treatment. The increase of the temperature of the preliminary annealing also increases the hardness of all alloys after HPT-treatment.

Published under license by AIP Publishing. <https://doi.org/10.1063/1.5053937>

I. INTRODUCTION

The Ti-alloys possess good corrosion resistance, low density, and high strength in a wide range of temperatures. They play an important role as materials for aircraft, building, and medicine. The structure and properties of titanium alloys can be tailored by a combination of mechanical and thermal treatments. Thus, severe plastic deformation (SPD) permits us to achieve very high strains in a material without its destruction. Moreover, SPD strongly changes the microstructure and properties of metallic alloys and also permits to tailor the properties of titanium-based alloys.¹⁻³ SPD is especially effective because titanium has various allotropic modifications, namely, the low-temperature α -phase, the high-temperature β -phase, as well as at high-pressure ω -phase.⁴⁻⁹

It is possible to achieve useful structural and property modifications of multicomponent and multiphase titanium-based alloys using the combination of preliminary heat treatment and high straining with high-pressure torsion (HPT) being one of the SPD modes. Recently, it was found that HPT not only leads to the grain refinement but also strongly accelerates bulk and grain-boundary phase transformations.¹⁰⁻¹⁴ In other words, the structure and composition of phases in a material after HPT differ from those before SPD.^{1,2,15} In particular, the high-pressure ω -phase appears in Ti-based alloys during HPT and is retained after pressure release.^{1,2} HPT also induces the formation and decomposition of supersaturated solid solutions as well as the evolution of α' -martensites.^{2,15}

The goal of this work is to understand how the composition and preliminary annealing of several Ti-V and Ti-V-Al alloys influence the formation of ω -phase and intermetallic particles during HPT, and how they change, in turn, the structure and hardness of these alloys [in the conventional processing without SPD, such alloys typically contain only one or two phases, namely α (with a hcp lattice) and β (with a bcc lattice)].^{16,17}

II. EXPERIMENTAL

To prepare the Ti-4 wt.% V, Ti-4 wt.% V-6 wt.% Al, Ti-4 wt.% V-3 wt.% Al, and Ti-5 wt.% V-6 wt.% Al alloys, pure titanium grade TI-1 (iodide titanium 99.98%), vanadium (99.98%), and aluminum (99.999%) have been used. Alloys were smelted in an induction furnace in an atmosphere of pure argon. The obtained ingots of alloys were structurally and chemically homogeneous over the entire length. Of the resulting cylindrical ingots of alloys with a diameter of 10 mm, the disks with a thickness of 0.6 mm were cut by spark erosion. The samples were then sealed in quartz ampoules and annealed in vacuum at a residual pressure of 4×10^{-4} Pa. After annealing, the samples were quenched in water together with ampoules. The annealing was carried out at temperatures of 600, 700, 900, and 950 °C, and the duration was 722, 168, 190, and 192 h, respectively. The annealed samples were subjected to HPT at room temperature at 7 GPa, deformation rate 1rpm, and 5 rotations of plunger in a Bridgman anvil type unit using a custom built computer-controlled device manufactured by W. Klement GmbH (Lang, Austria). After HPT, the thickness of the samples was 0.35 mm.

Microhardness measurements of the sample surface were carried out on a PMT-3 device. The Vickers diamond pyramid was used with a load of 50 g, the average number of measurements per sample was 10, and measurements were made in the region of half the radius of the sample. The measurement procedure is described in Ref. 18. Before measuring

the microhardness, the surface of the samples was polished using a diamond paste with a grain size of $1 \mu\text{m}$. X-ray diffraction (XRD) has been studied using a Siemens D-500 X-ray diffractometer with Cu-K α radiation. Phase analysis and calculation of lattice parameters were carried out with the help of the program PowderCell for Windows Version 2.4.08.03.2000 (Werner Kraus & Gert Nolze, BAM, Berlin). The thin sections of the samples for transmission electron microscopy (TEM) studies were prepared by standard techniques including mechanical polishing and etching with Ar ions. The specimens were studied on a JEM-2100 transmission electron microscope at 200 kV.

III. RESULTS AND DISCUSSION

Figure 1 shows the X-ray diffraction patterns for the Ti-4 wt.% V and Ti-4 wt.% V-6 wt.% Al alloys after annealing at 600 °C (bottom curves) and after HPT (top curves). XRD patterns show broadening and blurring of the peaks after HPT as well as a decrease in their intensity. It can be seen that the samples are strongly textured after annealing and HPT. For other investigated annealing temperatures, the XRD patterns demonstrate similar behavior. After annealing (at all investigated temperatures), both Ti-4 wt.% V and Ti-4 wt.% V-6 wt.% Al alloys contain two phases (α Ti) and (β Ti) (Table I, the data are also given for the Ti-4 wt.% V-3 wt.% Al, and Ti-5 wt.% V-6 wt.% Al alloys). A higher content of the (α Ti) phase is observed before HPT in the ternary Ti-4 wt.% V-6 wt.% Al alloy, whereas the amount of (β Ti) phase is very small there. After HPT, the (β Ti) phase completely disappears, and only one (α Ti) phase remains. The binary Ti-4 wt.% V alloy behaves differently. Namely, a high-pressure ω -phase appears after HPT in addition to the two available phases (α Ti) + (β Ti). However, the amount of a high-pressure ω -phase after HPT is quite small (about 2%-5%). Table I shows the data demonstrating that all three ternary alloys have a similar behavior in terms of phase composition before and after HPT. Thus, differently to the Ti-4 wt.% Fe and Ti-4 wt.% Co alloys,^{19,20} the

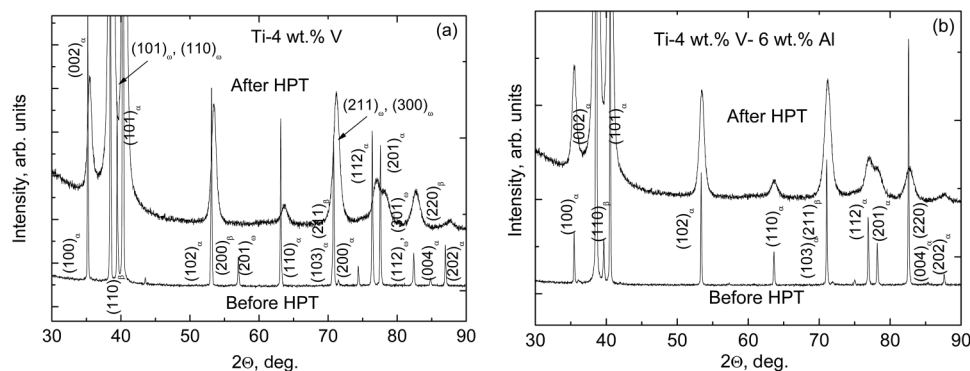


FIG. 1. X-ray diffraction patterns for (a) Ti-4 wt.% V and (b) Ti-4 wt.% V-6 wt.% Al alloys after annealing at 600 °C (lower patterns) and after HPT with preliminary heat treatment (upper patterns).

TABLE I. Phases and their amount in studied titanium alloys after annealing and after following HPT, where τ is the annealing time.

Alloys	T ($^{\circ}\text{C}$), τ (h)	The phases present in the sample after annealing before HPT	The phases present in the sample after HPT
Ti-4 wt. % V	600, 722 700, 168 950, 192	(αTi)hex—main phase, (βTi)cub—a noticeable amount	(αTi)hex—main phase, (βTi)cub—a noticeable amount, ω -фаза (hex)—low amount (few percent)
Ti-4 wt. % V-6 wt. % Al	600, 722 700, 168 950, 192	(αTi)hex—main phase, (βTi)cub—low amount	(αTi)hex—main phase
Ti-4 wt. % V-3 wt. % Al	600, 720 700, 240 900, 190	(αTi)hex—main phase, (βTi)cub—low amount	(αTi)hex—main phase
Ti-5 wt. % V-6 wt. % Al	600, 720 700, 240 900, 190	(αTi)hex—main phase, (βTi)cub—low amount	(αTi)hex—main phase

HPT of the Ti-4 wt. % V alloy produces only a very low amount of (ωTi) phase. Moreover, the addition of Al to the binary Ti-V alloys completely suppresses the formation of (ωTi) phase after HPT.

Figure 2 shows the bright-field TEM images and respective selected area electron diffraction (SAED) patterns for (a) Ti-4 wt. % V and (b) Ti-4 wt. % V-6 wt. % Al alloys after annealing at 700 $^{\circ}\text{C}$ and after HPT. SAED-patterns show the presence in the samples of more than one phase, and these phases are finely dispersed. Their nanoscale is confirmed by the absence of additional peaks on X-ray spectra. Small-size Moiré patterns also confirm the presence of a high density of nanoscale defects or precipitates of nanosized phases. Figures 2(d) and 2(e) show the radial intensity distributions respective to the diffraction patterns in (a) and (b). Intensities were integrated along the Debye rings. Blue bar charts show the positions of the reflections from (αTi). Green bar charts show the positions of the reflections from (βTi). The Ti-4 wt. % V alloy [Fig. 2(c)] contains after HPT mainly (αTi) with a small amount of (βTi) phase. The peaks of (ωTi) are not visible in TEM (most probably due to its low amount). The ternary Ti-4 wt. % V-6 wt. % Al alloy [Fig. 2(d)] contains after HPT mainly the (αTi) phase. However, in ternary Ti-4 wt. % V-6 wt. % Al alloy, the additional weak and broad peaks are also present in the radial intensity distributions. They are marked by arrows in Fig. 2(d) and may be attributed as ones from a titanium aluminide with tetragonal lattice, namely those of Ti_2Fe .

The more pronounced differences between the four studied alloys are seen in the temperature dependences of the lattice parameters a and c for the (αTi) phase (Figs. 3 and 4). The lattice parameters a and c decrease by the addition of 4 wt. % V to pure titanium. The increase of the annealing temperature leads to the slight decrease of parameters a and c (Fig. 4) in the (αTi) phase in Ti-4 wt. % V alloy. This

corresponds to the increasing solubility of vanadium in the (αTi) phase at the studied annealing temperatures.¹⁶ The addition of 6 wt. % Al to the binary Ti-4 wt. % V alloy leads to a further decrease of lattice parameters a and c for the (αTi) phase (Fig. 4). Parameter a is almost independent on the annealing temperature [Fig. 4(a)] and lattice parameter c in the Ti-4 wt. % V-6 wt. % Al alloy decreases with increasing annealing temperature [Fig. 4(b)]. In other two ternary alloys, the lattice parameters a and c for the (αTi) phase depend similarly on the annealing temperature (Fig. 3).

HPT leads to the change of the lattice parameters a and c for the (αTi) phase (Figs. 3 and 4). In the binary Ti-4 wt. % V alloy, both a and c remain almost unchanged. However, in the ternary Ti-4 wt. % V-6 wt. % Al alloy, the lattice parameters a and c increase after HPT and move toward those of pure titanium (Fig. 4). They become almost equal to those in the binary alloy without aluminum. This fact allows us to suppose that aluminum leaves the (αTi) phase. In any case, the lattice parameters become closer to those for pure titanium, and it means that HPT “purifies” the (αTi) phase in the ternary Ti-4 wt. % V-6 wt. % Al alloy. This behavior is very similar to the “purification” of (αTi) phase and ($\alpha'\text{Ti}$) martensite after HPT observed recently in the binary Ti-Fe alloys.²

Where can the aluminum (and possibly also vanadium) atoms migrate during HPT from the (αTi) phase? The first answer is that they move into the remaining trace amount of the (βTi) phase. The (βTi) phase can accommodate much more aluminum and vanadium atoms than (αTi) due to the high solubility of Al and V in (βTi).¹⁶ However, the amount of (βTi) phase after HPT is very low. The second answer is that they are used to form extremely fine particles of titanium aluminide visible in TEM in the radial intensity distributions [Fig. 2(d)]. The third answer is connected with new grain boundaries (GBs). It is well known that HPT leads to the strong grain refinement.^{3,21–29} The grain size in the annealed samples before HPT is several hundreds of micrometers and after HPT it becomes three orders of magnitude lower. Therefore, a lot of new GBs form during the HPT. All these new grain boundaries should contain segregation layers. It is known that GB segregation in nanograined materials can strongly increase the overall solubility of the second component.³⁰ Thus, the second explanation of “purification” of (αTi) phase is that the aluminum (and possibly also vanadium) atoms are consumed by the segregation layers formed during HPT. Such behavior has been recently observed for steels where the lattice of (αFe) also can accommodate only few carbon atoms.³¹ In any case, during the “purification” of the (αTi) phase in the Ti-4 wt. % V-6 wt. % Al, the mass-transfer takes place, and the aluminum (and possibly also vanadium) atoms leave the bulk of the (αTi) grains. This HPT-induced diffusion-like mass transfer proceeds extremely quick, like in other Ti-based alloys,^{1,2} and the estimated equivalent diffusion coefficients are 10–15 orders of magnitude higher than the bulk diffusion coefficient extrapolated to 300 K (being the HPT temperature).⁴ And it is despite the fact that the applied pressure additionally slows down the diffusion process.^{32,33}

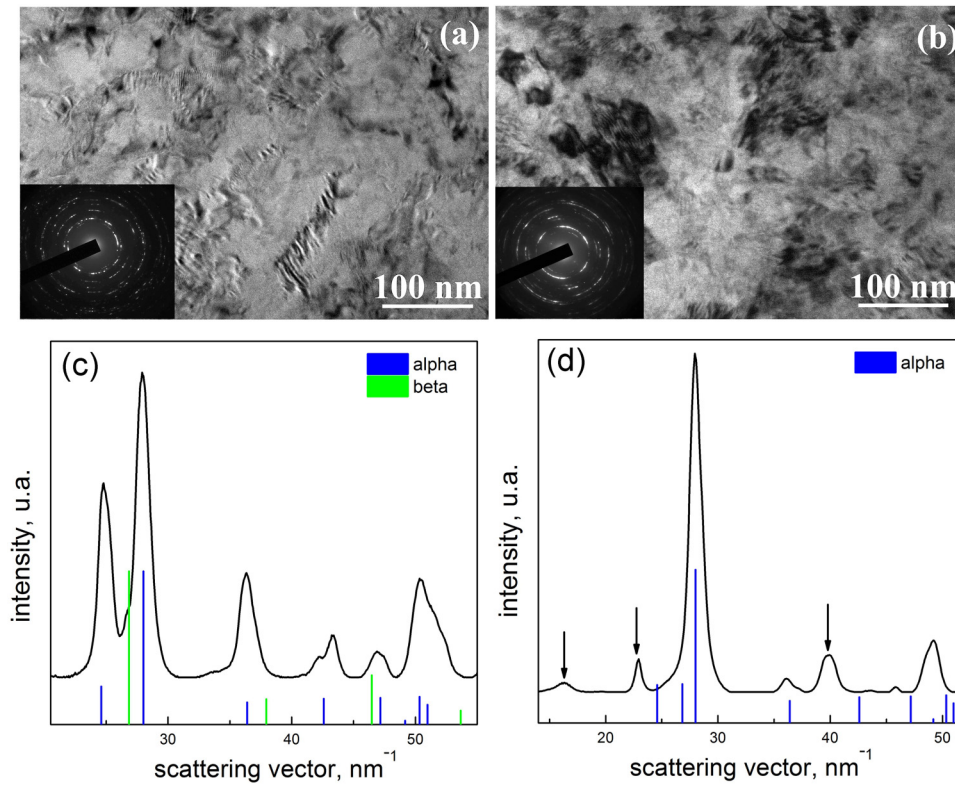


FIG. 2. Bright-field TEM micrographs for (a) Ti-4 wt. % V and (b) Ti-4 wt. % V-6 wt. % Al alloys after annealing at 700 °C and after HPT. The insets in (a) and (b) show selected area electron diffraction patterns. (c) and (d) Radial intensity distributions respective to the diffraction patterns in (a) and (b). Intensities were integrated along the Debye rings. Blue bar charts show the positions of the reflections from (α Ti). Green bar charts show the positions of the reflections from (β Ti). Arrows in (d) show the additional peaks from one of the titanium aluminides with tetragonal lattice, most probably Ti_2Fe .

Some mechanical characteristics of pure phases in titanium are known from the literature. In Ref. 34, the elastic moduli were measured in a coarse-crystalline Ti-4 wt. % V-6 wt. % Al for the α and β -phases. It was experimentally shown

that the elastic modulus of the α phase is 22% larger than that of the β phase. It was shown in Ref. 35 that the shear modulus of the β -phase decreases with increasing annealing temperature in the range from 600 to 975 °C. In a theoretical

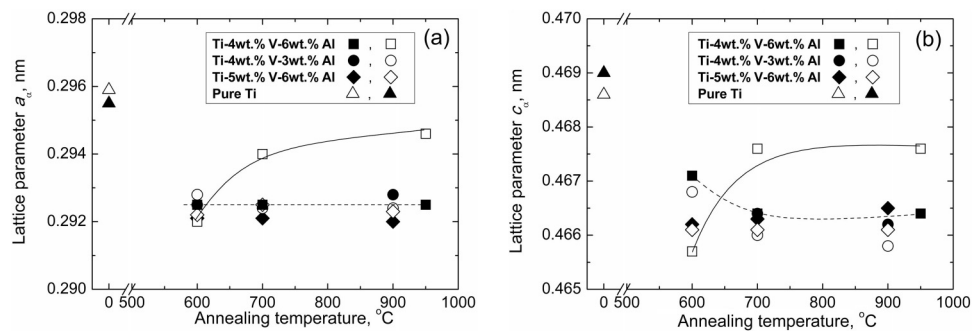


FIG. 3. Temperature dependences of lattice parameters a (a) and c (b) in (α Ti) phase in pure Ti,² Ti-4 wt. % V-6 wt. % Al, Ti-4 wt. % V-3 wt. % Al, and Ti-5 wt. % V-6 wt. % Al alloys after annealing at 600, 700, 900, and 950 °C (filled symbols) and after HPT with preliminary heat treatment (open symbols). Lines are the guides for the eye.

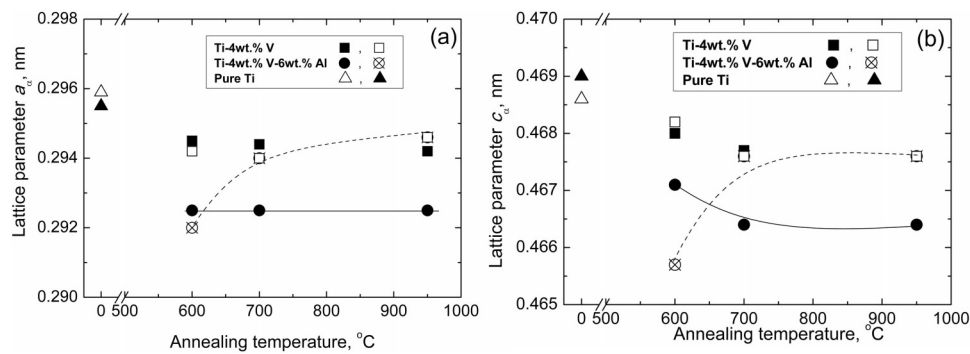


FIG. 4. Temperature dependences of lattice parameters a (a) and c (b) in (α Ti) phase in pure Ti,² Ti-4 wt. % V-6 wt. % Al, and Ti-4 wt. % V after annealing at 600, 700, and 950 °C (filled symbols) and after following HPT with preliminary heat treatment (open symbols). Lines are the guides for the eye.

paper,³⁶ it was shown that the specific energy of the α/β interfacial boundary decreases by a factor of two with increasing temperature.

Figure 5 shows microhardness values after HPT with preliminary heat treatment. From Fig. 5, we see two features: (1) the microhardness of the Ti-4 wt. % V alloy is higher than that of the Ti-4 wt. % V-6 wt. % Al alloy, and both temperature dependences have a minimum at $T = 700$ °C; (2) For alloys Ti-4 wt. % V-3 wt. % Al and Ti-5 wt. % V-6 wt. % Al after annealing and HPT, the microhardness dependences have a linear form, and the microhardness increases with an increase of the annealing temperature by more than 10%. The first feature, as we assume, can be explained by the dispersion hardening, namely, by the presence of two additional (β Ti) and (ω Ti) phases which are not present in the ternary alloy. Therefore, the hardness values for the binary alloy are higher than those for all three-component alloys in the investigated temperature range.

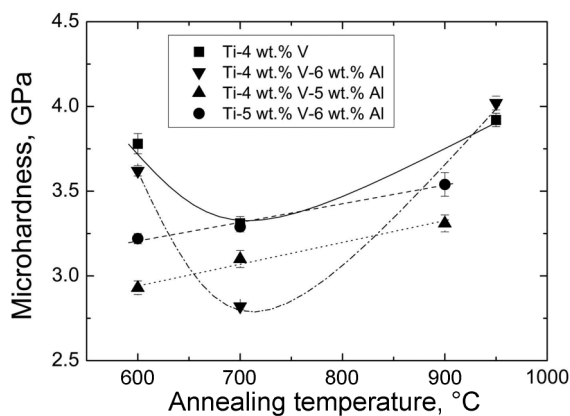


FIG. 5. Dependence of microhardness of Ti-4 wt. % V, Ti-4 wt. % V-6 wt. % Al, Ti-4 wt. % V-3 wt. % Al, and Ti-5 wt. % V-6 wt. % Al alloys after HPT on the temperature of preliminary annealing.

The second feature, as we assume, can be related to the morphology of the original structure, namely, the phenomenon of “grain boundary wetting a second solid-phase.” Earlier, the phenomenon of “grain boundary wetting a second solid-phase” was studied in detail in two-component alloys, including titanium alloys.^{37,38} In these studies, we observed the phenomenon of “wetting” of (α Ti)/(α Ti) grain boundaries by the second solid phase (β Ti). The fraction of the completely “wetted” grain boundaries depends on the annealing temperature. At 600 °C, the portion of “wetted” boundaries is close to zero, and at 700–800 °C, it reaches its maximum of more than 50% and higher. This allows us to assume that the more the (α Ti)/(α Ti) grain boundaries are replaced by the interlayer the second solid phase (β Ti), the weaker is the grain refinement at HPT, since the (β Ti)-phase is less elastic than the (α Ti) one, and therefore the hardness after annealing at $T = 700$ °C and HPT decreases.

IV. CONCLUSIONS

The applied straining by the high pressure torsion strongly influences both microstructure and properties of the studied titanium-based alloys. HPT strongly refines the grain size and induces the formation of the (ω Ti) phase in pure Ti and binary Ti-4 wt. % V alloy. The comparative analysis of the Ti-4 wt. % V, Ti-4 wt. % V-6 wt. % Al, Ti-4 wt. % V-3 wt. % Al, and Ti-5 wt. % V-6 wt. % Al alloys subjected to HPT with preliminary heat treatment showed a strong influence of the third component, namely aluminum. The addition of aluminum leads to the (1) suppression of the formation of the (β Ti) as well as (ω Ti) phases and (2) change in the lattice parameters a and c in (α Ti), especially in the Ti-4 wt. % V-6 wt. % Al alloy. The microhardness for all the investigated alloys increases with an increase in the annealing temperature.

ACKNOWLEDGMENTS

The authors are deeply grateful to M. I. Egorin (Material Science Laboratory, ISSP RAS) for the production of titanium

alloys and A. R. Kilmametov (Institute of Nanotechnologies KIT, Karlsruhe, Germany) for HPT sample processing. Sample preparation, microstructural studies, and microhardness measurements were carried out with the support of the Russian Federation for Basic Research (RFBR) grant (Project No. 16-03-00285). Torsion under high pressure was carried out with the support of the RFBR grant (Project No. 16-53-12007). The support of the Ministry of Education and Science of the Russian Federation in the framework of the Program to Increase the Competitiveness of NUST "MISIS" and agreement No. 14.B25.31.0018 is acknowledged.

REFERENCES

- ¹A. Kilmametov, Y. Ivanisenko, A. A. Mazilkin, B. B. Straumal, A. S. Gornakova, O. B. Fabrichnaya, M. J. Kriegel, D. Rafaja, and H. Hahn, *Acta Mater.* **144**, 337 (2018).
- ²A. Kilmametov, Y. Ivanisenko, B. Straumal, A. A. Mazilkin, A. S. Gornakova, M. J. Kriegel, O. B. Fabrichnaya, D. Rafaja, and H. Hahn, *Scr. Mater.* **136**, 46 (2017).
- ³R. Z. Valiev, R. K. Islamgaliev, and I. Alexandrov, *Prog. Mater. Sci.* **45**, 103 (2000).
- ⁴M. J. Donachie, Jr., *Titanium: A Technical Guide*, 2nd ed. (ASM International, Materials Park, OH, 2000).
- ⁵D. Errandonea, Y. Meng, M. Somayazulu, and D. Häusermann, *Physica B* **355**, 116 (2005).
- ⁶D. R. Trinkle, R. G. Hennig, S. G. Srinivasan, D. M. Hatch, M. D. Jones, H. T. Stokes, R. C. Albers, and J. W. Wilkins, *Phys. Rev. Lett.* **91**, 025701 (2003).
- ⁷S. K. Sikka, Y. K. Vohra, and R. Chidambaram, *Prog. Mater. Sci.* **27**, 245 (1982).
- ⁸S. Banerjee and P. Mukhopadhyay, *Phase Transformations Examples from Titanium and Zirconium Alloy* (Elsevier, Amsterdam, 2010).
- ⁹B. S. Hickman, *J. Mater. Sci.* **4**, 554 (1969).
- ¹⁰V. G. Gavriljuk, *Mater. Sci. Eng. A* **345**, 81 (2003).
- ¹¹X. Sauvage, F. Wetscher, and P. Pareige, *Acta Mater.* **53**, 2127 (2005).
- ¹²B. B. Straumal, X. Sauvage, B. Baretzky, A. A. Mazilkin, and R. Z. Valiev, *Scr. Mater.* **70**, 59 (2014).
- ¹³B. Straumal, A. Korneva, and P. Zięba, *Arch. Civil Mech. Eng.* **14**, 242 (2014).
- ¹⁴B. B. Straumal, A. R. Kilmametov, Y. Ivanisenko, A. A. Mazilkin, O. A. Kogtenkova, L. Kurmanaeva, A. Korneva, P. Zięba, and B. Baretzky, *Int. J. Mater. Res.* **106**, 657 (2015).
- ¹⁵B. B. Straumal, A. R. Kilmametov, A. Korneva, A. A. Mazilkin, P. B. Straumal, P. Zięba, and B. Baretzky, *J. Alloys Comp.* **707**, 20 (2017).
- ¹⁶*Binary Alloy Phase Diagrams*, edited by T. B. Massalski (American Society for Metals, Metals Park, OH, 1991).
- ¹⁷H. Wang, N. Warnken, and R. C. Reed, *Mater. Sci. Eng. A* **528**, 622 (2010).
- ¹⁸I. E. Permyakova, A. M. Glezer, and K. V. Grigorovich, *Bull. Russ. Acad. Sci. Phys.* **78**, 996 (2014).
- ¹⁹B. B. Straumal, A. R. Kilmametov, Y. Ivanisenko, A. A. Mazilkin, R. Z. Valiev, N. S. Afonikova, A. S. Gornakova, and H. Hahn, *J. Alloys Comp.* **735**, 2281 (2018).
- ²⁰A. R. Kilmametov, Y. Ivanisenko, B. B. Straumal, A. S. Gornakova, A. A. Mazilkin, and H. Hahn, *Metals* **8**, 1 (2018).
- ²¹W. Lojkowski, M. Djahanbakhsh, G. Burkle, S. Gierlotka, W. Zielinski, and H. J. Fecht, *Mater. Sci. Eng. A* **303**, 197 (2001).
- ²²C. M. Cepeda-Jiménez, J. M. García-Infanta, A. P. Zhilyaev, O. A. Ruano, and F. Carreño, *J. Alloys Comp.* **509**, 636 (2011).
- ²³Y. Ivanisenko, W. Lojkowski, R. Z. Valiev, and H. J. Fecht, *Acta Mater.* **51**, 5555 (2003).
- ²⁴V. V. Sagaradze and V. A. Shabashov, *Nanostruct. Mater.* **9**, 681 (1997).
- ²⁵S. Ohsaki, S. Kato, N. Tsuji, T. Ohkubo, and K. Hono, *Acta Mater.* **55**, 2885 (2007).
- ²⁶A. V. Sergueeva, C. Song, R. Z. Valiev, and A. K. Mukherjee, *Mater. Sci. Eng. A* **339**, 159 (2003).
- ²⁷S. D. Prokoshkin, I. Y. Khmelevskaya, S. V. Dobatkin, I. B. Trubitsyna, E. V. Tatyannin, V. V. Stolyarov, and E. A. Prokofiev, *Acta Mater.* **53**, 2703 (2005).
- ²⁸X. Sauvage, L. Renaud, B. Deconihout, D. Blavette, D. H. Ping, and K. Hono, *Acta Mater.* **49**, 389 (2001).
- ²⁹T. Miyazaki, D. Terada, Y. Miyajima, C. Suryanarayana, R. Muraio, Y. Yokoyama, K. Sugiyama, M. Umamoto, T. Todaka, and N. Tsuji, *J. Mater. Sci.* **46**, 4296 (2011).
- ³⁰B. B. Straumal, S. G. Protasova, A. A. Mazilkin, E. Goering, G. Schütz, P. B. Straumal, and B. Baretzky, *Beilstein J. Nanotechnol.* **7**, 1936 (2016).
- ³¹Y. Ivanisenko, X. Sauvage, A. Mazilkin, A. Kilmametov, J. A. Beach, and B. B. Straumal, *Adv. Eng. Mater.* **20**, 1800443 (2018).
- ³²D. A. Molodov, B. B. Straumal, and L. S. Shvindlerman, *Scr. Metall.* **18**, 207 (1984).
- ³³D. A. Molodov, J. Swiderski, G. Gottstein, W. Lojkowski, and L. S. Shvindlerman, *Acta Metall. Mater.* **42**, 3397 (1994).
- ³⁴E. A. Trofimov, R. Y. Lutfullin, and R. M. Kashaev, *Lett. Mater.* **5**, 67 (2015).
- ³⁵J. W. Elmer, T. A. Palmer, S. S. Babub, and E. D. Specht, *Mater. Sci. Eng. A* **391**, 104 (2005).
- ³⁶M. A. Murzinova, S. V. Zhrebtsov, and G. A. Salishchev, *J. Exp. Theor. Phys.* **122**, 705 (2016).
- ³⁷A. S. Gornakova, S. I. Prokofiev, K. I. Kolesnikova, and B. B. Straumal, *Russ. J. Non-Ferr. Met.* **56**, 229 (2016).
- ³⁸A. S. Gornakova, B. B. Straumal, A. N. Nekrasov, A. Kilmametov, and N. S. Afonikova, *J. Mater. Eng. Perform.* **27**, 4989 (2018).